



**Novel Graphene-Like Nanosheets Supported Highly Active
Electrocatalysts with Ultralow Pt Loadings for Oxygen
Reduction Reaction**

Journal:	<i>Journal of Materials Chemistry A</i>
Manuscript ID:	TA-ART-07-2014-003704.R1
Article Type:	Paper
Date Submitted by the Author:	13-Aug-2014
Complete List of Authors:	Li, Zesheng; Sun Yat-sen University, Li, Yunyong; Sun Yat-Sen University, Jiang, San Ping; Curtin University of Technology, Department of Chemical Engineering He, Guoqiang; Sun Yat-sen University, Shen, Pei; Sun Yat-sen University,

Cite this: DOI: 10.1039/c0xx00000x

PAPER

www.rsc.org/xxxxxx

Novel Graphene-Like Nanosheets Supported Highly Active Electrocatalysts with Ultralow Pt Loadings for Oxygen Reduction Reaction

Zesheng Li^{a,§}, Yunyong Li^{a,§}, San Ping Jiang^{b,*}, Guoqiang He^c and Pei Kang Shen^{a,*}

⁵ Received (in XXX, XXX) Xth XXXXXXXXX 200X, Accepted Xth XXXXXXXXX 200X

DOI: 10.1039/b000000x

A novel active graphene-like nanosheet (AGN) with high specific surface area is firstly developed as efficient electrocatalyst support synthesized through an efficient ion-exchange-assisted synthesis route. The AGN shows a high electronic conductivity and strong cohesive force and distribution effect toward
10 the catalyst nanoparticles. The AGN supported Pd_xPt_y bimetallic catalyst system with ultralow Pt loadings exhibits excellent catalytic performance and superb durability for the oxygen reduction reaction of fuel cells, giving a high mass activity of 1930 mA mg⁻¹_{Pt} at 0.9 V vs. RHE.

Introduction

In the past decades, advanced catalysts based on supported nanoparticles (NPs) have been demonstrated to be highly active and stable in different types of catalytic reactions involving chemical catalysis and electrocatalysis aspects.¹ Supported precious metal NPs currently are one of the most feasible electrocatalysts for fuel cells because of their optimized usage of the metal NPs and reduction in material cost.² To achieve a high performance fuel cell catalyst, the catalyst support should meet the requirements of excellent electronic conductivity, high corrosion resistance, high surface area and strong cohesive force toward catalyst particles.³ Currently, graphene-based carbon materials including monolayer and multilayer nanosheets are highly promising as the new-generation supporting material for electrocatalysts, owing to their high specific surface area, high electronic conductivity, and outstanding chemical and electrochemical stability.⁴ However, the intrinsic hydrophobic properties of graphitized basal plane structures cause a great difficulty in uniformly loading metal NPs on the surface of graphene.⁵ Though the hydrophilicity of the reduced graphene oxide (RGO) could be improved via introducing oxygen functional groups, their electronic conductivity is still insufficient due to their partly restored graphitic structures.⁶ Based on this fact, it is of fundamental interest to develop the novel graphene-based carbon materials with high specific surface area, high electronic conductivity as well as strong affinity to foreign constituents, beyond the continuous development of hybrid architectures for electronics and various electrochemical systems.⁷

The development of electrocatalysts with low Pt loading is a constant theme in response to the worldwide deficiency in Pt resource. This typically requires the control of nanoparticle structure and the increased utilization of Pt through alloying or core-shell approaches. Noble metal-based bimetallic alloy NPs (e.g. PdPt⁸, AgPt⁹ and AuPt¹⁰ NPs) with small size (~5 nm), have recently received increasing attention in electrocatalysis applications ranging from oxidation of small organic molecules (methanol, formic acid) to oxygen reduction reactions (ORR). Both the decreased dimension and heterogeneous metal constitution have contributed to their excellent catalytic properties and the durability of the systems.¹¹ For fuel cells, cathodic ORR plays an essential role in producing electricity and is a major limiting factor on fuel cell performance. Currently, the development of high-performance ORR electrocatalysts with low Pt loading is a pivotal process to step up the commercialization of fuel cells.¹² As one promising candidate for designing low Pt loading alloyed catalysts, Pd manifests several advantages including its lattice good match with Pt,¹³ inherent ORR activity in the acidic medium,¹⁴ and its affordable price along with worldwide availability.¹⁵ However, the Pt content in previous reported PdPt alloy catalysts is still very high (about 1/5 in mass),⁸ so it is of necessity to further reduce the content of Pt via the Pt skin structure, so as to producing efficient ultra-low Pt loading electrocatalysts for the oxygen reduction reactions.¹⁶ The hybridisation of functionalized graphene with Pt-based NPs has been developed and further improvement achieved in catalytic performance for these low Pt electrocatalysts.¹⁷ However, there are several key issues while designing the

practical electrocatalysts still need to be addressed: (i) The functionalizing graphene often requires addition of specified coupling reagents¹⁸, which will decrease the electrical conductivity and even bring instability of the electrochemical systems; (ii) The distribution uniformity and dimensional controllability of mostly reported Pt alloy NPs on pristine graphene are barely satisfactory and thus far from the high catalytic performance and optimized utilization efficiency¹⁹; and (iii) The complex process and high cost of production will be potential obstacles for the universal use of above graphene-alloy NPs in technological fields²⁰. Therefore, it is desirable to overcome the limitations of these hybrid architectures and thus create opportunities for their popularization in practical applications.

Herein, we propose a new type of functionalized 2-D carbon materials, active graphene nanosheets (AGNs), which will integrate the aforementioned design principles. The highly graphitized structures and relatively high specific surface area have been simultaneously achieved for our product, synthesized via a synchronous graphitization-activation combination method using a functional ion-exchange-resin as carbon precursor [see Experimental section for details]. As a feasible supporting material for electrocatalysts, these AGNs are designed on the basis of the following considerations: (i) the highly graphitized structure ensures good electrical conductivity for the established catalyst system; (ii) the high specific surface area provides adequate location for accommodating the catalyst particles; (iii) the well hydrophilicity of active graphite materials allows strong cohesive force and distribution effect to the catalyst particles; and (iv) the facile and scalable fabricated method illustrates a good prospect of application and extension. On the base of this novel support, we successfully constructed an ultra-low Pt loading AGNs-Pd₁₀Pt₁ bimetallic catalysts (mass ratio of Pd and Pt is 10:1, in Pt skin structure). For this hybrid system, three features have become apparent over previous reports:¹⁷⁻²⁰ (i) A one-step growth route was applied to uniformly deposit small Pd₁₀Pt₁ bimetallic NPs onto the graphene nanosheets, and the Pt skin structure was caused by the H₂ heat treatment [see Experimental section for details]; (ii) The content of Pt among the alloy has been reduced to a ultra-low level (below 1/10 in mass), which is an inspired attempt to the design of low-Pt-loading catalysts system; (iii) Highly active and stable electrocatalysts for the oxygen reduction reaction of fuel cells has been demonstrated on the basis of the novel hybrid architectures.

Experimental

Synthesis of the AGNs.

The AGNs was synthesized via a synchronous graphitization-activation combination method, by using an ion-exchange resin as carbon precursor, nickel acetate as catalyst of graphitization and KOH as reagent of activation. Typically, the pretreated macroporous acrylic type cation exchange resin (1 kg, Shanghai Hualing Resin Co., Ltd, China) was impregnated with targeting ions in 10 L nickel acetate (Shanghai Hebao Chemical Co., Ltd, China) solution with concentration of 0.05 mol L⁻¹ for 6 h. The exchanged resin was washed with deionized water and dried at 80

°C for 12 h. Then the exchanged resin (100 g) was added in a 2 L KOH/ethanol solution containing 100 g KOH and stirred at 80 °C until the mixture solution became an ‘ink-paste’, followed by another 6 h of static soaking in ambient conditions. After that, the mixture solution was dried in the vacuum condition at 80 °C for 48 h and then smashed by a disintegrator. Finally, the mixture was heated at 800 °C for 2 h in N₂ atmosphere, with a heating rate of 2 °C min⁻¹ and an N₂ flow of 100 cc min⁻¹. After cooling down to room temperature, the resulting sample was added into 3 mol L⁻¹ HCl solution with a specific volume for more than 12 h with intensive sonication. Afterwards, the sample was repeatedly washed by deionized water until a pH value of 7 was reached, dried at 80 °C in ambient for 12 h.

Synthesis of Pd₁₀Pt₁/AGNs catalyst.

A one-step *in situ* growth route was applied to uniformly deposit small Pd₁₀Pt₁ bimetallic NPs onto the surface of AGNs. Typically, a certain amount of AGNs powders were added into a mixture of H₂PtCl₄, PdCl₂, sodium citrate, and glycol solution to form a uniform suspension in ultrasonic bath for 30 min. The pH of the suspension was adjusted to 10 by a 5 wt% NaOH/glycol solution. The sample was then put into a homemade programmable microwave oven (1000 W, 2.45 GHz) for heating in a 5 s on and 5 s off procedure for 20 times. Afterwards, the product was washed 5 times and dried in a H₂ Flow at 80 °C for 24 h.

Characterization.

The X-ray diffraction (XRD) measurements were carried out in a D/Max-III (Rigaku Co., Japan) using CuK α radiation with a scanning rate of 8° min⁻¹, operating at 40 kV and 30 mA. The transmission electron microscopic (TEM) investigations were carried out in a JEOL JEM-2010 (HR) at 200 kV. Scanning electron microscopy (SEM) pictures were collected on a JEM-6700F field emission scanning electron microscope. X-ray photoelectron spectroscopy (XPS) was conducted with two separate systems equipped with monochromatic Al K sources (ESCALab250, USA) to analyze the chemical composition of the samples. N₂ adsorption experiments using an ASAP 2420 Surface Area Analyzer (Micromeritics Co., USA) were conducted to investigate the specific surface area and porosity of the samples. And the inductively coupled plasma-atomic emission spectrometry (ICP-AES) was used to analyze the metal content of the as-attained samples (the total metal content is 32.04 wt.% (29.19 wt.% Pd + 2.85 wt.% Pt)).

The oxygen reduction reaction (ORR) was conducted on a PARE TAT 2273 instrument (Princeton Applied Research, USA) in the thermostat-controlled standard three-electrode cell at 25 °C using a rotating Pt ring and glassy carbon disk (6 mm in diameter) electrode, a home-made reversible hydrogen electrode (RHE) and a platinum foil (1.0×1.0 cm²) as the working electrode, reference electrode and counter electrode, respectively. The ORR measurement was carried out in an oxygen-saturated 0.1 mol/L HClO₄ solution scanned between 0.05 V and 1.20 V with a scan rate of 5 mV/s and a rotation speed of 1600 rpm. The kinetic current was calculated from the polarization curve by considering the mass-transport correction and normalized with respect to the mass of metal in order to compare the mass activity

(i_m) for different catalysts, according to the Levich-Koutecky equation: $1/i = 1/i_k + 1/i_d$ (where i is the experimentally obtained current, i_k the kinetic current and i_d the diffusion-limiting current).

Results and discussion

The crystallographic structures of the samples including RGO, AGNs, and Pd₁₀Pt₁/AGNs are examined by X-ray powder diffraction (XRD), as shown in Fig. 1. Comparison with RGO sample indicates that the (002) peak of the AGNs has a markedly increased intensity and is extremely aculeated at higher 2-theta angle, indicating the well graphitic structure of our product. The XRD pattern of Pd₁₀Pt₁/AGNs shows that the Pd₁₀Pt₁ NPs have the face centered cubic (fcc) structures with clear (111), (200), (220) and (311) facets. According to the Scherer's Equation²¹, the average particle sizes calculated from diffraction peak of (111) and (220) were 4.4 nm and 3.8 nm, respectively.

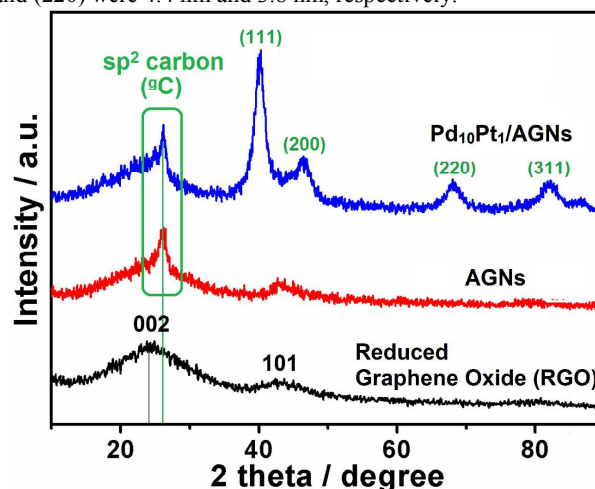


Fig. 1 XRD pattern of the samples: (blue) Pd₁₀Pt₁/AGNs, (red) AGNs and (black) reduced graphene oxide (RGO).

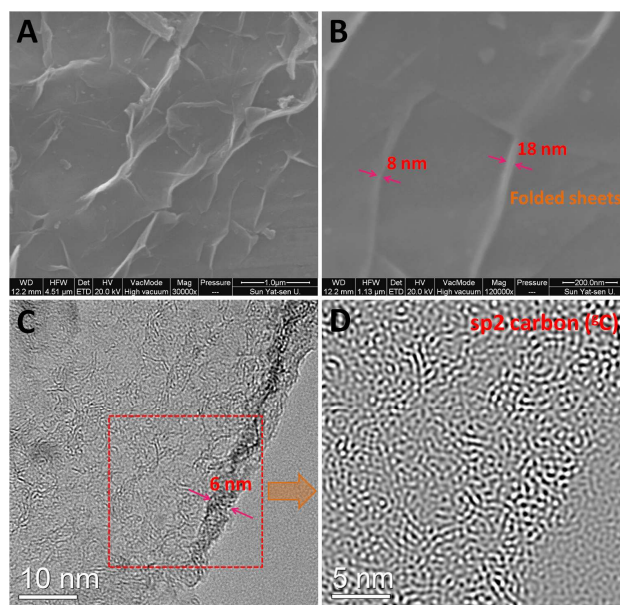


Fig. 2 (A and B) SEM micrographs and (C and D) TEM images of the as-prepared AGNs.

The typical morphology and microstructure of the as-prepared AGNs are examined by scanning electron microscopy (SEM) and transmission electron microscopy (TEM). From the SEM micrographs (Fig. 2 A and B), it can be observed that these AGNs are overlapped and crumpled with a dimension from several hundred nanometers to several micrometers with the thickness under 10 nm. The TEM image (Fig. 2C) further confirmed that the thickness of the sheet was about 6 nm, and a high-resolution TEM (HR-TEM) image (Fig. 2D) clearly showed the presence of a porous-network composed of highly curved, predominantly 2–5 layers graphitic carbon (^{13}C). Importantly, this sp^2 -bonded graphitic carbon (see the XRD result) with an interrelated 3-D structure guarantees a high electrical conductivity of the active graphite materials.²² A higher powder conductivity of the AGNs sample (1350 S m^{-1}), while that is only 460 S m^{-1} for the RGO sample, was measured by the four point probe technique. The Brunauer-Emmett-Teller (BET) specific surface area and the average adsorption pore size of the AGNs were $1143.8 \text{ m}^2 \text{ g}^{-1}$ and 4.12 nm , respectively (Fig. 3). All these results demonstrate that the combined graphitization and activation technique provided not only the well graphitic structures (resulting the high conductivity) but also the high surface area of the as-prepared graphene material.

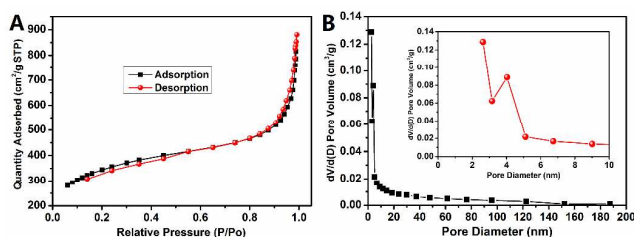


Fig. 3 Nitrogen adsorption-desorption isotherm (A) and pore-size distribution (B).

Morphologies of the bimetallic $\text{Pd}_{10}\text{Pt}_1$ nanoparticles assembled on AGNs have been characterized by the TEM. Fig. 4 shows the typical TEM images of the as-synthesized $\text{Pd}_{10}\text{Pt}_1/\text{AGNs}$ hybrid architectures. It is clear that a large-area and transparent AGN is uniformly decorated by the nanosized $\text{Pd}_{10}\text{Pt}_1$ particles with very few aggregations as shown in Fig. 4A–C, indicating a strong interaction between graphene support and metal nanoparticles. The moderate oxygen functional groups of AGNs would improve the hydrophilicity of the prepared carbon materials (Fig. 5), and thus endowing the catalyst particles with desirable distribution. The higher magnification TEM images selected from square frame of Fig. 4C indicate that several $\text{Pd}_{10}\text{Pt}_1$ NPs are linearly assembled into interesting rod-like one-dimensional (1-D) nanostructures (see Fig. 4D). The 1-D nanostructure of the noble metal is very attractive for electrocatalysis application, and the controlled experiment for these nanorod-like nanostructures is in progress. The various fringes from Fig. 4E demonstrate the single-crystal structures of these $\text{Pd}_{10}\text{Pt}_1$ nanocrystals. Fig. 4F is the inverse Fourier transform (IFT) image from Fig. 4E based on carbon, displaying the same sp^2 -bonded carbon (^{13}C) as shown in Fig. 2D. A HR-TEM image of two coterminous $\text{Pd}_{10}\text{Pt}_1$ NPs (see Fig. 4G) reveals

that the two nanocrystals have the same lattice spacing between (111) planes of 0.225 nm . The inset shows the corresponding Fast Fourier Transform (FFT) of this high-resolution image. Fig. 4H is the IFT image from Fig. 4G based on nanocrystals which shows an evident crystal dislocation (see the arrow). As a result, a distinct three-step twin boundary is readily observed from Fig. 4I for the two nanocrystals. These diversified structures of crystallographic plane are predicted to be of an affinity with the superior catalytic properties of metallic catalysts.²³ The various fringes from Fig. 4E demonstrate the single-crystalline structure of these $\text{Pd}_{10}\text{Pt}_1$ nanocrystals. The average size of these $\text{Pd}_{10}\text{Pt}_1$ NPs was calculated to be 4.2 nm by the TEM measurements that is in accordance with that of XRD analysis (see Fig. S1). The composition and metal content of the catalysts have been determined by energy-dispersive X-ray spectroscopy (EDS) and inductively coupled plasma-atomic emission spectrometry (ICP-AES) techniques. The analysis of EDS (see Fig. S2) based on a selected area TEM image shows that the mass ratio of Pd and Pt is 9.36 , which is a little lower than that of ICP-AES analysis (10.24). The results suggest that most Pt component has been enriched on the outer layer of the $\text{Pd}_{10}\text{Pt}_1$ NPs (Pt skin is formed), due to the heat treatment process in a H_2 flow at $80 \text{ }^\circ\text{C}$ for 24 h .

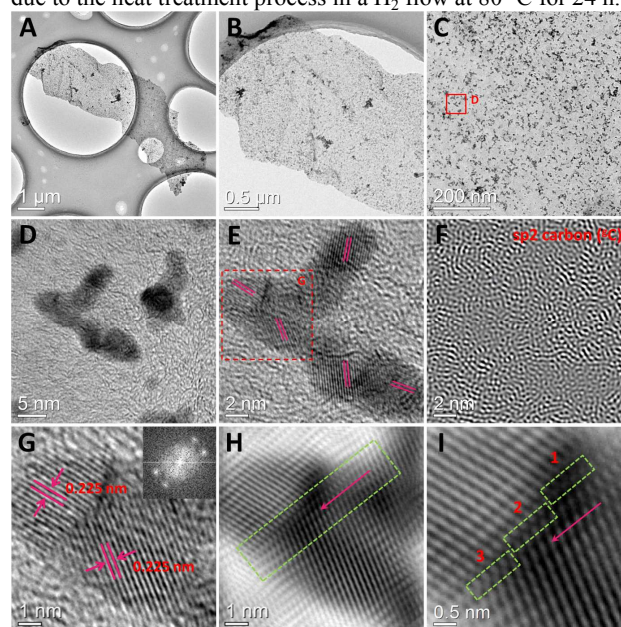


Fig. 4 TEM characterization of $\text{Pd}_{10}\text{Pt}_1/\text{AGNs}$: (A–C) lower and (D–F) higher magnification TEM images, (G–I) HR-TEM images, (F) inverse Fourier transform from (E) based on carbon and (H and I) inverse Fourier transform from (G) based on nanocrystals. Inset in (G) shows the Fast Fourier Transform image from (G).

The X-ray photoelectron spectroscopy (XPS) analysis (Fig. 5 A–C) of AGNs sample demonstrated that the Surface Atoms Content of C, O, and N are $86.89 \text{ At.}\%$, $10.57 \text{ At.}\%$, and $2.54 \text{ At.}\%$, respectively. The moderate oxygen functional groups of AGNs prepared by chemical activation would improve the hydrophilicity of the carbon materials. As shown in Fig. 5 D, 5 g AGNs sample can be uniformly dispersed in 1000 ml water without deposition after 48 h .

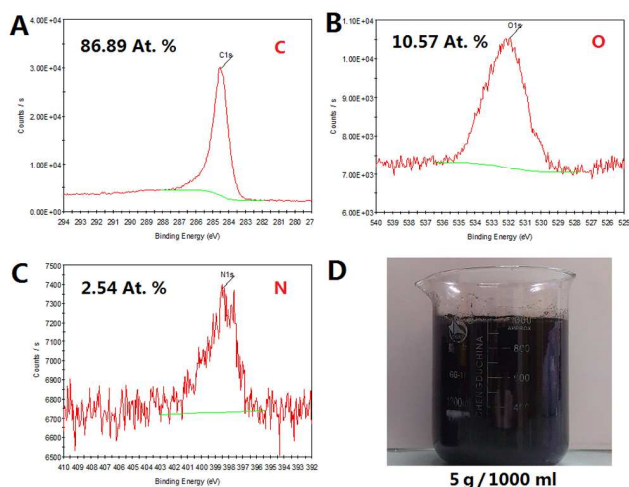


Fig. 5 XPS patterns (A-C) of the AGNs sample; Picture of AGNs-water solution (D).

To demonstrate the ORR activity and stability of the AGNs-Pd₁₀Pt₁ hybrid catalyst, the ORR polarization curves and cyclic voltammetric (CV) curves (before and after 10,000 cycles) at room temperature (28 °C) were obtained in O₂-saturated and N₂-saturated 0.1 M HClO₄ aqueous solution, respectively. Fig. 6A shows the ORR curves at a scan rate of 5 mV s⁻¹ and a rotation rate of 1600 rpm, which displays that the three curves are almost coincident before and after 1,000 and 10,000 CV cycles. Their onset potential is the same at 1.002 V (vs. RHE) and the half-wave potential difference is only 6 mV after 10,000 cycles. It is worthy to note that distinct hydrogen adsorption peak can be observed before 0.05 V in ORR curve, as a result of the high Pd content of the Pd₁₀Pt₁/AGNs catalyst. This should become one signal of the low-Pt-loading for present catalyst system¹³. The inset in Fig. 6A shows the CV curves, which were precycled at a scan rate of 200 mV s⁻¹ between 0.6 and 1.2 V (vs. RHE), that active area of the Pd₁₀Pt₁/AGNs catalyst does not decrease so obvious before and after 10,000 CV cycles. Based on the total metal content of 32.04 wt.% (29.19 wt.% Pd + 2.85 wt.% Pt), the mass activity (*i*_m) of the catalysts at 0.9 V as defined by the DOE²⁴ was determined based on Pt metal content and the results were depicted in Fig. 6B. Remarkably, the *i*_m values at 0.9 V based on Pt are calculated as high as 1930, 1795 and 1550 mA mg⁻¹_{Pt} before and after 1,000 and 10,000 CV cycles, as shown in the inset of Fig. 6B. It is clear that the percentage decreased is very limited. The Pt-mass activity of this low-Pt-content system significantly goes beyond the DOE target in 2017 (440 mA mg⁻¹_{Pt})²⁴. Remarkably, the catalytic performances concerning activity and stability of the present catalyst system are much superior to the commercial Pt/C catalyst (see Fig. S4) and even superior to some of the state-of-the-art low-Pt-loading catalyst systems.²⁵

In the past decade, our group and many others worldwide have demonstrated that Pd electrocatalysts are highly active in alkaline electrolyte solution.¹⁵ Remarkably, one of our latest investigation suggested that the inherent ORR activity of Pd in the acidic medium can be improved considerably by the promoted effect of support materials.¹⁴ In an attempt to clarify the promoted effect of the AGNs toward the metal active component, the single Pd/AGNs and Pt/AGNs catalyst are prepared and evaluated compared with those supported by commercial carbon (Vulcan

XC-72) (Fig. 7 A and B). The Pd/AGNs catalyst shows a large limiting diffusion current (over 5 mA cm⁻²) and a high on-set potential (0.97 V), but the results are poor for the Pd/Vulcan XC-72. The *i*_m@0.9 V of Pd/AGNs is 74 mA mg⁻¹_{Pd} in 0.1 M HClO₄ solution that is 4 times of the Pd/Vulcan XC-72 (18.5 mA mg⁻¹_{Pd}).

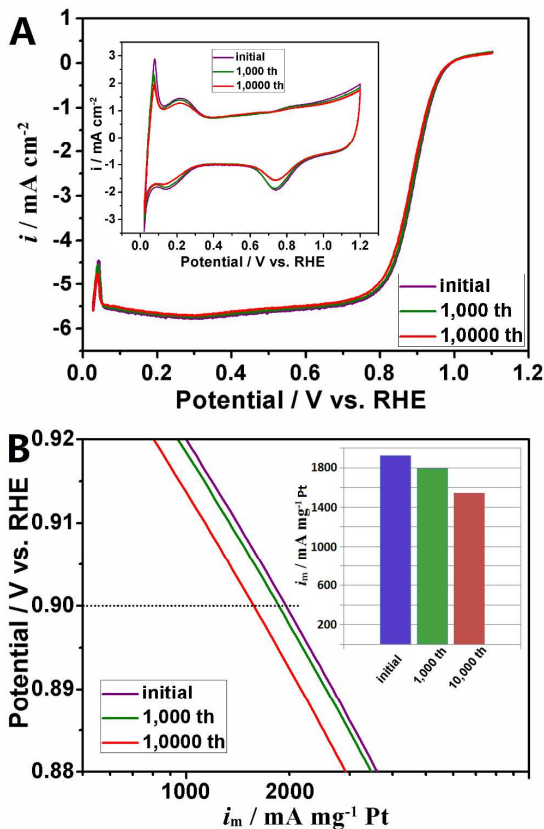


Fig. 6 Electrochemical performance of the Pd₁₀Pt₁/AGNs catalyst: (A) ORR polarization curves, the inset is the CV curves, (B) mass activities based on Pt metal, the inset compares the mass activities at 0.9 V at different stages.

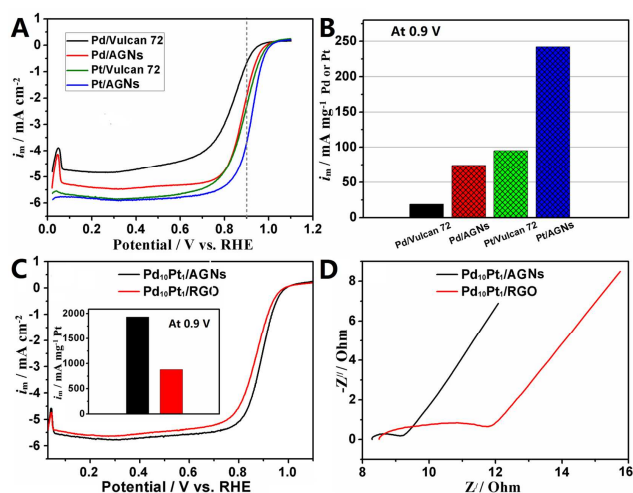
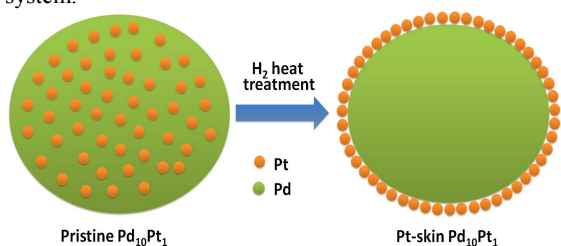


Fig. 7 (A) ORR curves (B) mass activities of the single metal samples; (C) ORR curves of Pd₁₀Pt₁/RGO and Pd₁₀Pt₁/AGNs, and (D) Nyquist plots obtained from the EIS of Pd₁₀Pt₁/RGO and Pd₁₀Pt₁/AGNs.

Table 1 Catalytic activity for various catalysts ($i_m@0.9$ V, mA $\text{mg}^{-1}_{\text{Pt}}$).

Samples	Pd ₁₁ Pt ₁ /AGNs	Pd ₁₀ Pt ₁ / AGNs	Pd ₉ Pt ₁ / AGNs	Pd ₈ Pt ₂ / AGNs	Pd/A GNs	Pt/A GNs
Before H ₂ heat treatment	429	455	460	478	74	242
After H ₂ heat treatment	1812	1930	1820	975	---	242

At the same time, the $i_m@0.9$ V of Pt/AGNs catalyst is 242 mA $\text{mg}^{-1}_{\text{Pt}}$, which is almost 2.5 times of the Pt/Vulcan XC-72 (96 mA $\text{mg}^{-1}_{\text{Pt}}$). Therefore, the promoted effect of Pd component and AGNs should be the fundamental cause of the high performance for the Pd₁₀Pt₁/AGNs catalyst. On the other hand, after subtraction of the contribution of Pd (74 mA $\text{mg}^{-1}_{\text{Pd}}$), the $i_m@0.9$ V of Pt component in Pd₁₀Pt₁ is still as high as 1185 mA $\text{mg}^{-1}_{\text{Pt}}$. This enhancement mainly benefits from the alloy and Pt-skin structures of the Pd₁₀Pt₁ bimetallic catalyst in addition to the supporting effect of AGNs. And that the systematical investigation of Pd₁₁Pt₁, Pd₁₀Pt₁, Pd₉Pt₁, Pd₈Pt₂ catalysts (mass ratios) on the AGNs indicated that the Pd₁₀Pt₁/AGNs catalyst is of the optimized catalytic activity on Pt among the series of bimetallic structures (see Table 1). The heat treatment process in H₂ atmosphere would be an effective strategy for preparation of Pt skin nanostructures, which have been well demonstrated in previous work.²⁶ Therefore, it is important to note that the H₂ heat treatment is also the crucial factor for the highly improved catalytic activity, since the Pt-skin structure of Pd₁₀Pt₁ NP was probably formed (see Scheme 1). Likewise, the H₂ heat treatment has been proved to be an assurance of the catalytic stability of the system.²⁶

**Scheme 1** Illustration of the formation of Pt skin Pd₁₀Pt₁ nanostructure.

For the sake of comparison, Pd₁₀Pt₁/RGO catalyst with the same loading was also prepared with RGO as a support. Fig. 7 C shows the ORR performances of Pd₁₀Pt₁/RGO and Pd₁₀Pt₁/AGNs, and the Fig. 7 D shows their Nyquist plots obtained from the electrochemical impedance spectroscopy (EIS). The $i_m@0.9$ V of the Pd₁₀Pt₁/RGO catalysts is only 870 mA $\text{mg}^{-1}_{\text{Pt}}$ (Fig. 7 C), which is much lower than that (1930 mA $\text{mg}^{-1}_{\text{Pt}}$) of Pd₁₀Pt₁/AGNs catalysts. The larger semicircles (larger charge transfer resistance (CTR)) and the larger x-intercept (larger equivalent series resistance (ESR)) were observed for Pd₁₀Pt₁/RGO (3.64 Ω for CTR, 8.50 Ω for ESR), whereas only small semicircle and x-intercept were shown for Pd₁₀Pt₁/AGNs (0.87 Ω for CTR, 8.28 Ω for ESR) (Fig. 7 D). Therefore, it is reasonable that the

Pd₁₀Pt₁/AGNs catalyst system shows much higher activity than the Pd₁₀Pt₁/RGO catalyst system, due to the better electronic conductivity of the AGNs.

Based on above discussion, the Pt-based mass activity for Pd₁₀Pt₁ is much higher than that of the DOE target in 2017, while, the mass activity based on platinum group metal (PGM, Pt+Pd) total content is lower than that of the DOE target in 2017. However, We believe that the mass activity based on PGM would be much enhanced by further structural adjustment, for instance, by the design of multi-component AgPt@Pt core shell nanostructure on the active graphene-like nanosheet (AGN). Further work is in progress.

Conclusions

In summary, we have proposed a novel AGNs as one of the feasible supporting materials for electrocatalysts, which is characterized by highly graphitized structure, high specific surface area, good electronic conductivity and improved hydrophilicity. The development of the AGNs is based on a high-efficiency graphitization-activation integrated technique, manifesting a good prospect of large-scale production for practical applications. On the base of this novel material, an ultra-low Pt loading electrocatalysts of Pd₁₀Pt₁/AGNs hybrid system was successfully fabricated. Due to the remarkable supporting effect of AGNs and favorable bimetallic structure, a highly active and stable electrocatalysts for the oxygen reduction reaction in fuel cells has been demonstrated. It is highly expected that the design and synthesis of AGNs-supported metallic structures is a viable route to fabricate practical Pt-based electrocatalysts with ultra-low Pt loading, high activity and high durability to significantly reduce the cost of fuel cell systems.

Acknowledgments.

This work was supported by the Major International (Regional) Joint Research Project (51210002), the link project of the National Natural Science Foundation of China and Guangdong Province (U1034003), the National Natural Science Foundation of China (21073241), the Specialized Research Fund for the Doctoral Program of Higher Education of China (20110171110024), and Australian Research Council (DP120104932).

Notes and references

^a The State Key Laboratory of Optoelectronic Materials and Technologies, School of Physics and Engineering, Sun Yat-sen University, Guangzhou, 510275, PR China. E-mail: stsspk@mail.sysu.edu.cn; Tel. +86-20-84036736; Fax. +86-20-84113369

^b Fuels and Energy Technology Institute & Department of Chemical Engineering, Curtin University, Perth, WA6102, Australia. E-mail: s.jiang@curtin.edu.au; Tel. +61 8 9266 9804; Fax. +61 8 9266 1138.

^c College of Materials Science and Engineering, Guangxi University, Nanning, Guangxi, 530004, PR China.

[†] Those authors contributed equally.

[‡] Those authors contributed equally.

- †Electronic Supplementary Information (ESI) available: [details of any supplementary information available should be included here]. See DOI: 10.1039/b000000x/
- 5 1 (a) M. Chen, Y. Cai, Z. Yan, D. W. Goodman, *J. Am. Chem. Soc.*, 2006, **128**, 6341-6346; (b) Q. Liu, J. C. Bauer, R. E. Schaak, J. H. Lunsford, *Angew. Chem.*, 2008, **120**, 6317-6320; (c) E. A. Anumol, P. Kundu, P. A. Deshpande, G. Madras, N. Ravishankar, *ACS Nano*, 2011, **5**, 8049-8061.
- 10 2 (a) S. T. Kuk.; A. Wieckowski, *J. Power Sources*, 2005, **141**, 1-7; (b) H. Wang, R. Wang, H. Li, Q. Wang, J. Kang, Z. Lei, *Int. J. Hydrogen Energy*, 2011, **36**, 839-848.
- 3 (a) Y. Wang, D. Wilkinson, J. Zhang, *Chem. Rev.*, 2011, **111**, 7625-7651; (b) X. Chen, G. Wu, J. Chen, X. Chen, Z. Xie, X. Wang, *J. Am. Chem. Soc.*, 2011, **133**, 3693-3695.
- 15 4 (a) V. K. Prashant, *J. Phys. Chem. Lett.*, 2011, **2**, 242-251; (b) Y. Liang, Y. Li, H. Wang, J. Zhou, J. Wang, T. Regier, H. Dai, *Nat. Mater.* 2011, **10**, 780-786.
- 5 (a) S. Zhang, Y. Shao, H. Liao, M. Engelhard, G. Yin, Y. Lin, *ACS Nano*, 2011, **5**, 1785-1791; (b) J. Seo, A. Green, A. Antaris, M. Hersam, *J. Phys. Chem. Lett.*, 2011, **2**, 1004-1008.
- 20 6 (a) D. Cai, M. Song, *J. Mater. Chem.*, 2010, **20**, 7906-7915; (b) S. Chen, W. Cai, R. Piner, J. Suk, Y. Wu, Y. Ren, J. Kang, R. Ruoff, *Nano Lett.*, 2011, **11**, 3519-3525.
- 25 7 (a) X. Huang, X. Qi, F. Boey, H. Zhang, *Chem. Soc. Rev.*, 2012, **41**, 666-686; (b) S. Bai, X. Shen, *RSC Adv.*, 2012, **2**, 64-98; (c) L. Dai, *Acc. Chem. Res.*, 2013, **46**, 31-42; (d) D. Chen.; H. Feng.; J. Li, *Chem. Rev.*, 2012, **112**, 6027-6053.
- 8 (a) W. Wang, Q. Huang, J. Liu, Z. Zou, Z. Li, H. Yang, *Electrochem. Commun.*, 2008, **10**, 1396-1399; (b) Y. Liu, M. Chi, V. Mazumder, K. More, S. Soled, J. Henao, S. Sun, *Chem. Mater.*, 2011, **23**, 4199-4203.
- 30 9 (a) K. Kim, K. Kim, K. Shin, *J. Phys. Chem. C*, 2011, **115**, 23374-23380; (b) Y. Feng, L. Bi, Z. Liu, D. Kong, Z. Yu, *J. Catalysis*, 2012, **290**, 18-25.
- 35 10 (a) B. Wanjala, J. Luo, R. Loukrakpam, B. Fang, D. Mott, P. Njoki, M. Engelhard, H. Naslund, J. Wu, L. Wang, O. Malis, C. Zhong, *Chem. Mater.*, 2010, **22**, 4282-4294; (b) G. Chen, Y. Li, D. Wang, L. Zheng, G. You, C. Zhong, L. Yang, F. Cai, J. Cai, B. Chen, *J. Power Sources*, 2011, **196**, 8323-8330.
- 40 11 Y. Bing, Liu, H. L. Zhang, D. Ghosh J. Zhang, *Chem. Soc. Rev.*, 2010, **39**, 2184-2202.
- 12 (a) H. Meng, P. K. Shen, *J. Phys. Chem. B*, 2005, **109**, 22705-22709; (b) C. Wang, N. Markovic, V. Stamenkovic, *ACS Catal.*, 2012, **2**, 891-898.
- 45 13 B. Lim, Jiang, J. M. P. Camargo, E. Cho, J. Tao, X. Lu, Y. Zhu, Y. Xia, *Science*, 2009, **324**, 1302-1305.
- 14 S. Yin, M. Cai, C. Wang, P. K. Shen, *Energy Environ. Sci.*, 2011, **4**, 558-563.
- 15 C. Bianchini, P. K. Shen, *Chem. Rev.*, 2009, **109**, 4183-4206.
- 50 16 K. Sasaki, H. Naohara, Y. Choi, Y. Cai, W. Chen, P. Liu, R. Adzic, *Nat. Commun.*, 2012, DOI: 10.1038/ncomms2124.
- 17 (a) S. Wang, X. Wang, S. Jiang, *Phys. Chem. Chem. Phys.*, 2011, **13**, 6883-6891; (b) S. Guo, S. Sun, *J. Am. Chem. Soc.*, 2012, **134**, 2492-2495.
- 55 18 (a) S. Zhang, Y. Shao, H. Liao, J. Liu, I. Aksay, G. Yin, Y. Lin, *Chem. Mater.*, 2011, **23**, 1079-1081; (b) J. Shi, G. Yang, J. Zhu, *J. Mater. Chem.*, 2011, **21**, 7343-7349.
- 19 (a) Y. Hu, H. Zhang, P. Wu, H. Zhang, B. Zhou, C. Cai, *Phys. Chem. Chem. Phys.*, 2011, **13**, 4083-4094; (b) H. Zhang, X. Xu, P. Gu, C. Li.; P. Wu, C. Cai, *Electrochim. Acta*, 2011, **56**, 7064-7070.
- 60 20 (a) J. Chai, F. Li, Y. Hu, Q. Zhang, D. Han, L. Niu, *J. Mater. Chem.*, 2011, **21**, 17922-17929; (b) S. Guo, S. Dong, E. Wang, *ACS nano* 2010, **4**, 547-555.
- 21 H. Wang, G. Yang, Q. Li, X. Zhong, F. Wang, Z. Li, Y. Li, *New J. Chem.*, 2011, **35**, 469-475.
- 65 22 Y. Zhu, S. Murali, M. D. Stoller, K. J. Ganesh, W. Cai, P. J. Ferreira, A. Pirkle, R. M. Wallace, K. A. Cychosz, M. Thommes, D. Su, E. A. Stach, R. S Ruoff, *Science*, 2011, **332**, 1537-1541.
- 23 C. Wang, D. Vliet, K. More, N. Zaluzec, S. Peng, S. Sun, H. Daimon.; G. Wang, J. Greeley, J. Pearson, A. Paulikas, G. Karapetrov, D. Strmcnik, N. Markovic, V. Stamenkovic, *Nano Lett.*, 2011, **11**, 919-926.
- 70 24 U. S. Department of Energy, Technical Plan: Fuel Cells, 2011 (http://www1.eere.energy.gov/hydrogenandfuelcells/mypp/pdfs/fuel_cells.pdf).
- 75 25 (a) J. Shui, C. Chen, C. M. Li, *Adv. Funct. Mater.*, 2011, **21**, 3357-3362; (b) J. Snyder, I. McCue, K. Livi, J. Erlebacher, *J. Am. Chem. Soc.*, 2012, **134**, 8633-8645; (c) C. Koenigsmann, E. Sutter T. Chiesa, R. Adzic, S. Wong, *Nano Lett.*, 2012, **12**, 2013-2020; (d) S. Alia, K. Jensen, B. Pivovar, Y. Yan, *ACS Catal.*, 2012, **2**, 858-863; (e) Z. Li, C. He, M. Cai, S. Kang, P. Shen, *Int. J. Hydrogen Energy*, 2012, **37**, 14152-14160.
- 80 26 D. Wang, H. Xin, R. Hovden, H. Wang, Y. Yu, D. Muller, F. DiSalvo, H. Abruña, *Nat. Mater.*, 2013, **12**, 81-87.
- 85

TOC:

The novel active graphene-like nanosheets supported ultralow Pt catalyst of Pd₁₀Pt₁ (Pt skin structure) nanoparticles have been made as highly active and stable catalysts for the oxygen reduction reaction.

